Electronic Supplementary Information

First Principles Study of Thermoelectric Performance in Pristine and Binary Alloyed Monolayers of Noble Metals

Table S1 DZP basis parameters optimized for bulk fcc structure, where V_{soft} and r_i are parameters for soft-confining potential. Cut-off radii for first and second zeta (radial part of wavefunction) are controlled by E_{shift} and split norm respectively.

Element	V_{soft} (in Ry)	Soft inner radii r_i	Energy Shift E_{shift} (in meV)	Split norm for $l = 0$	Split norm for $l = 1$
Au	86.15	0.78	19.64	0.15	0.40
Ag	88.69	0.95	20	0.29	0.33
Cu	191	0.99	20	0.35	0.29
Pt	20	0.95	20	0.15	0.40

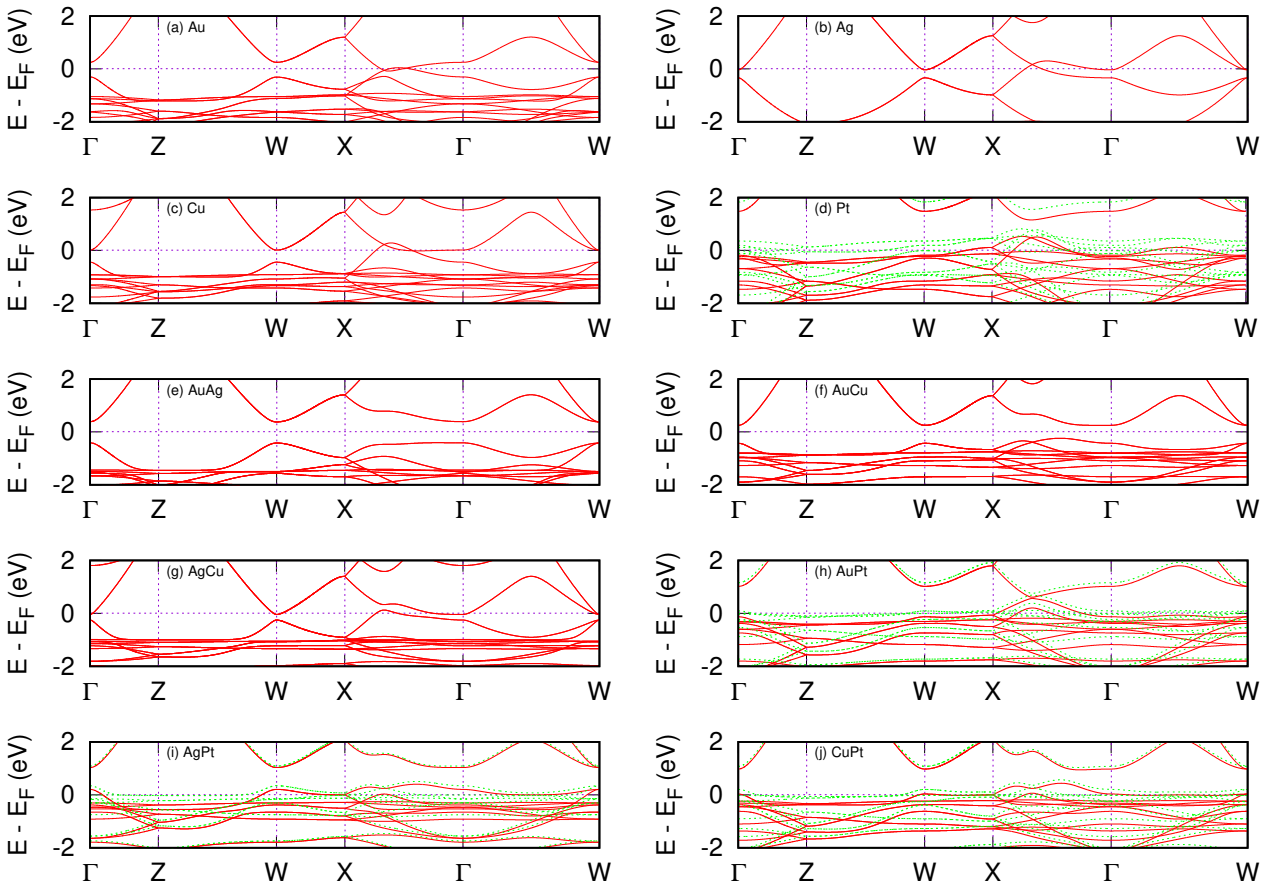

Figure S1 Electronic band structures of considered monolayers for (a-d) pristine monolayers, (e-g) non-magnetic alloyed monolayers, and (h-j) magnetic alloyed monolayers. In figures for pristine Pt and magnetic alloys, solid red lines represent bands for ↑-spin and dotted green lines for ↓-spin states.

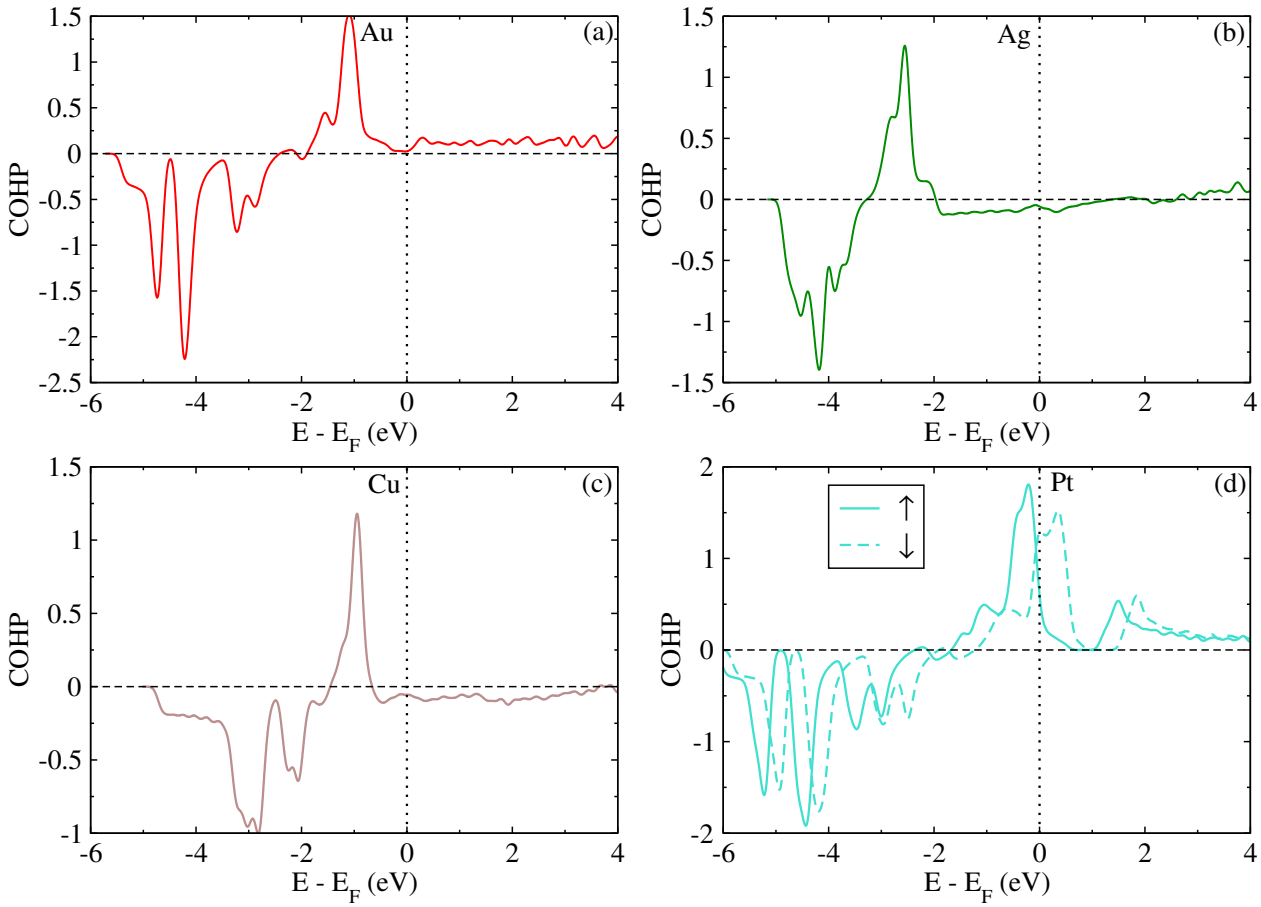

Figure S2 Crystal orbital hamiltonian population (COHP) curves for pristine monolayers.

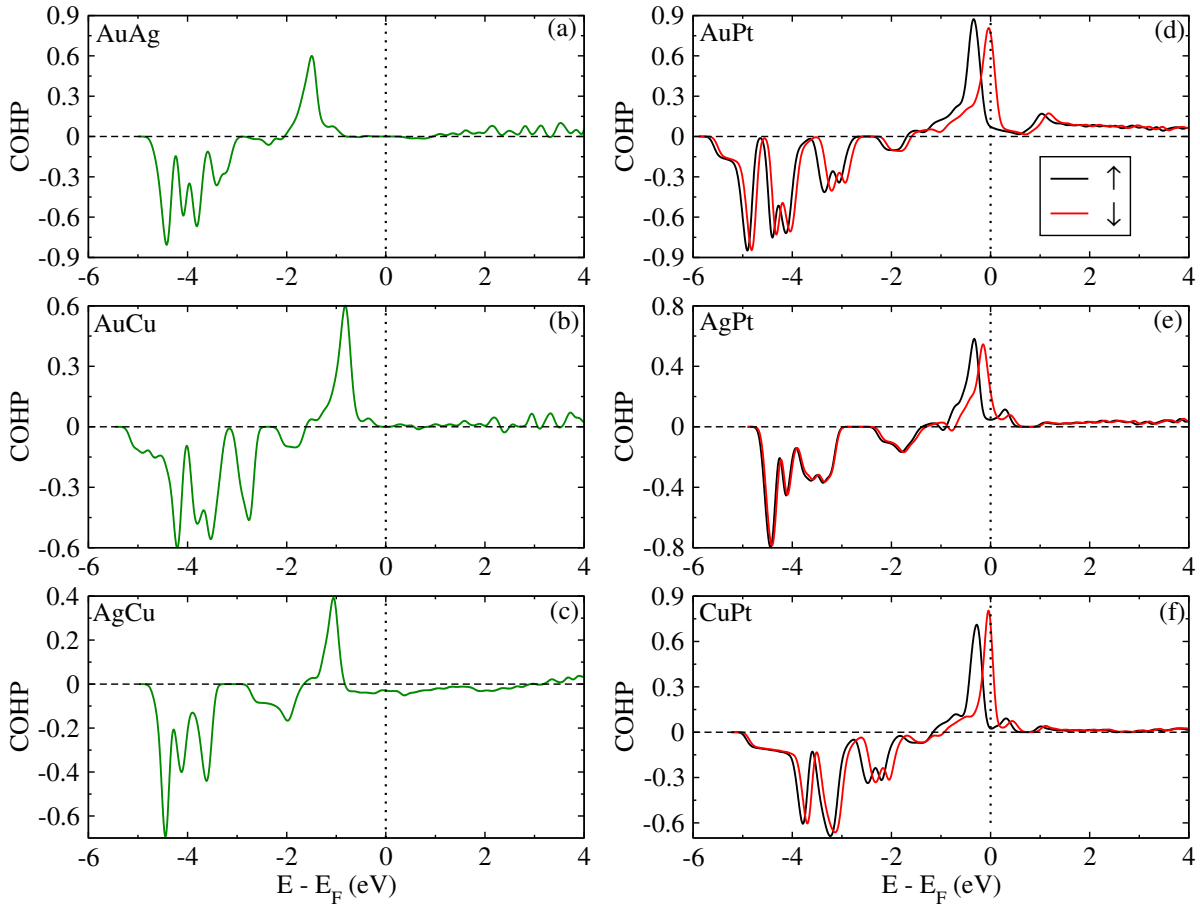

Figure S3 Same as in S2 for alloyed monolayers.

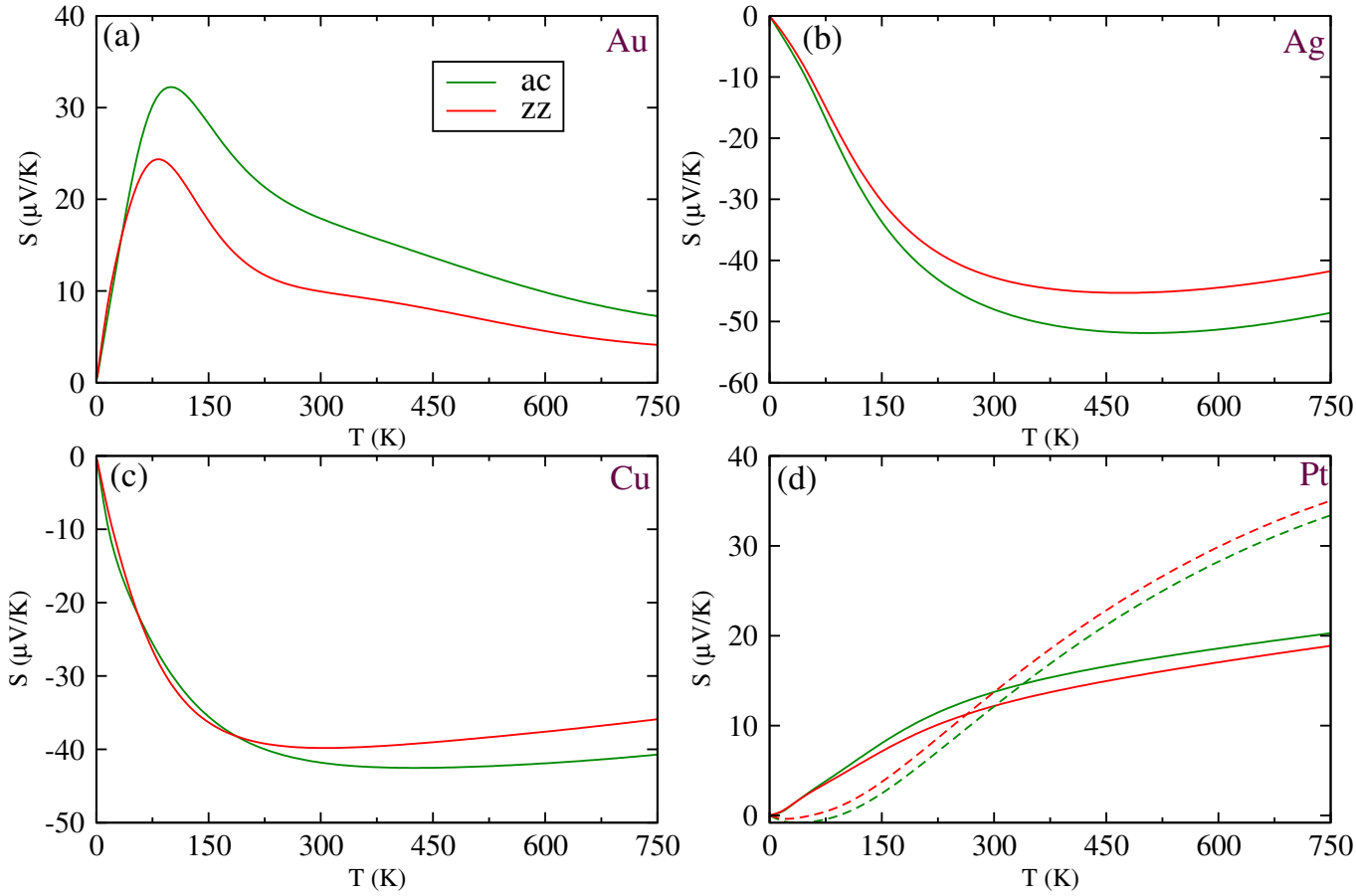

Figure S4 Temperature dependence of Seebeck-coefficient S under zero bias for pristine monolayers. Dashed lines in (d) represent the spin-Seebeck co-efficient for Pt monolayer.

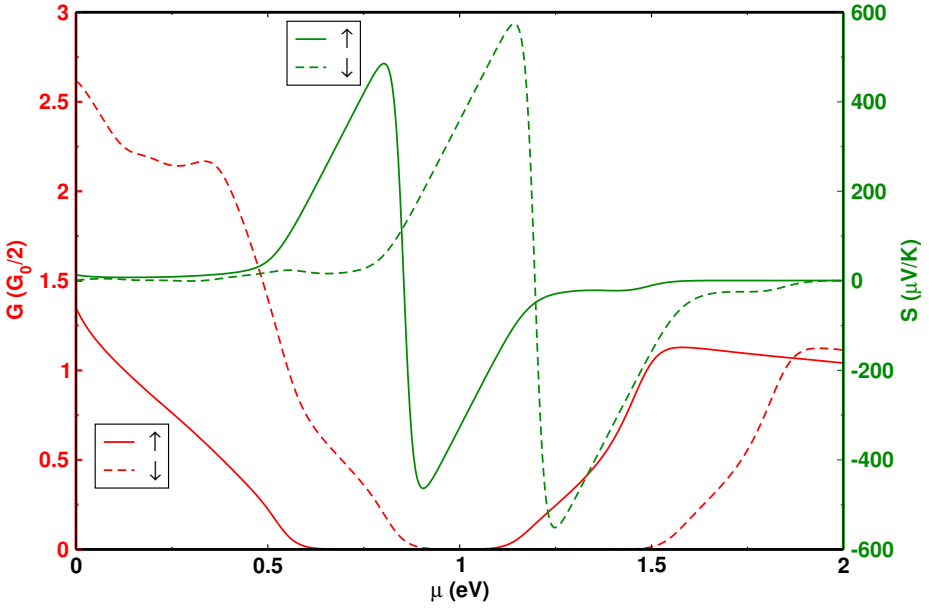

Figure S5 Tuning of spin-resolved G and S with chemical potential μ for Pt monolayer at room-temperature.

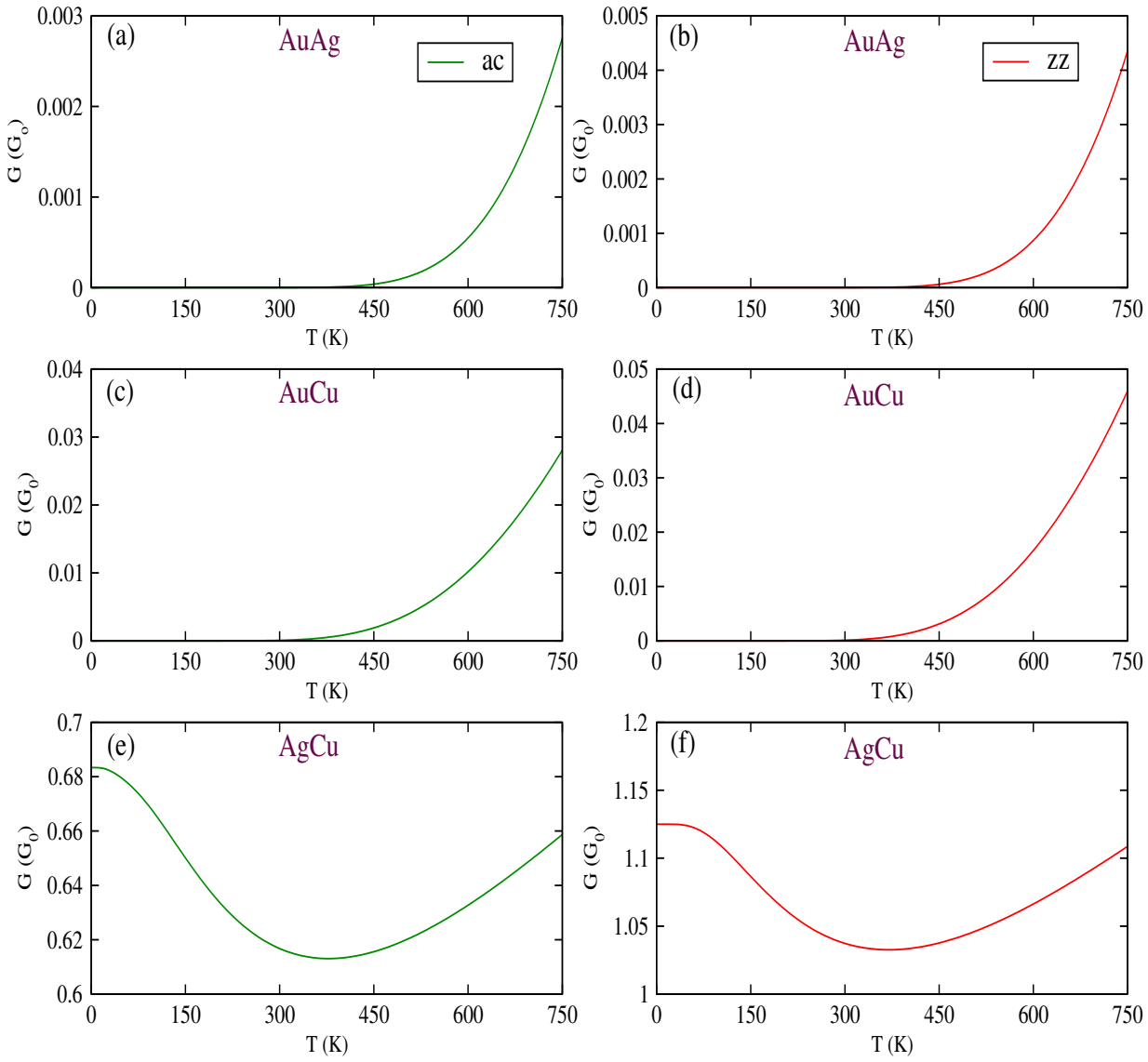

Figure S6 Calculated electrical conductance G as a function of temperature for AuAg, AuCu, and AgCu monolayers along the ac (zz) direction in left (right) column.

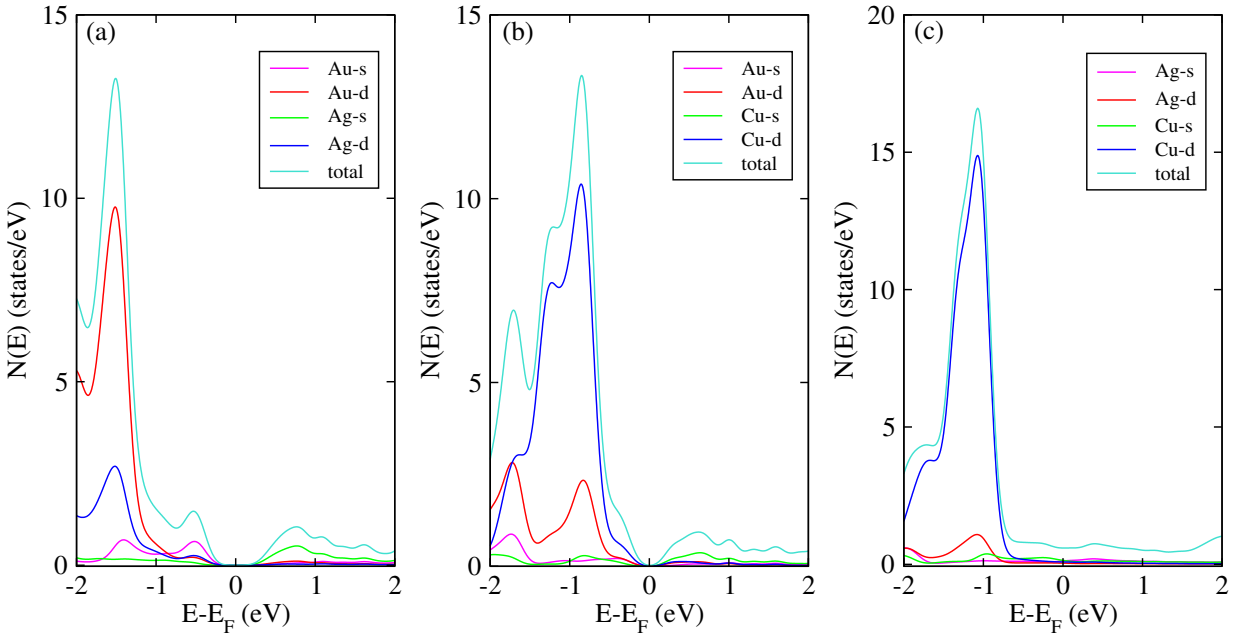

Figure S7 Orbital-resolved and total density of states for (a) AuAg, (b) AuCu, and (c) AgCu monolayers.

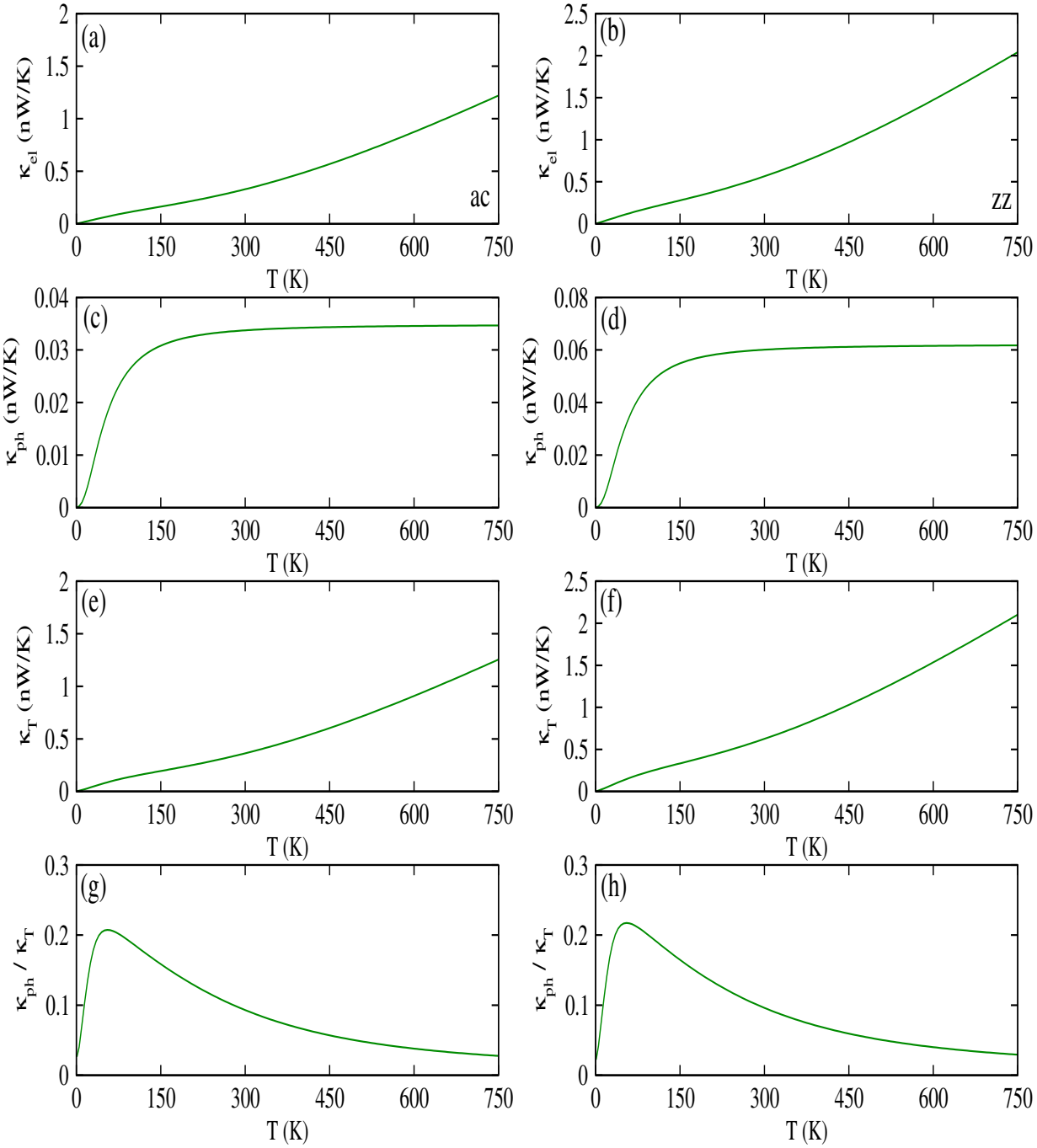

Figure S8 Variation of κ_{el}, κ_{ph}, κ_T, and κ_{ph}/κ_T with temperature for $\mu = 0$ in AgCu monolayer along ac (zz) direction in left (right) column.

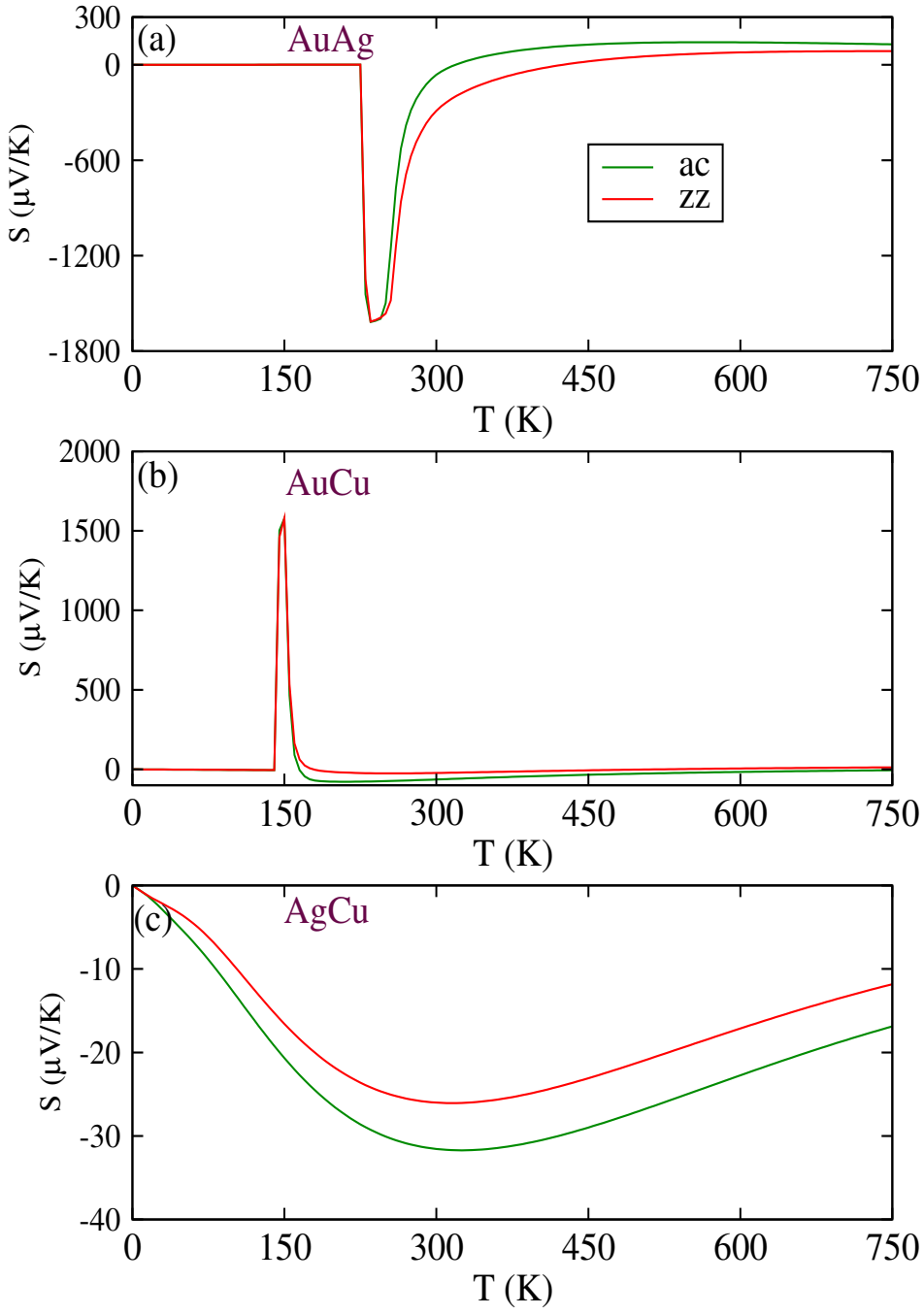

Figure S9 Same as in S4 for non-magnetic alloyed monolayers.

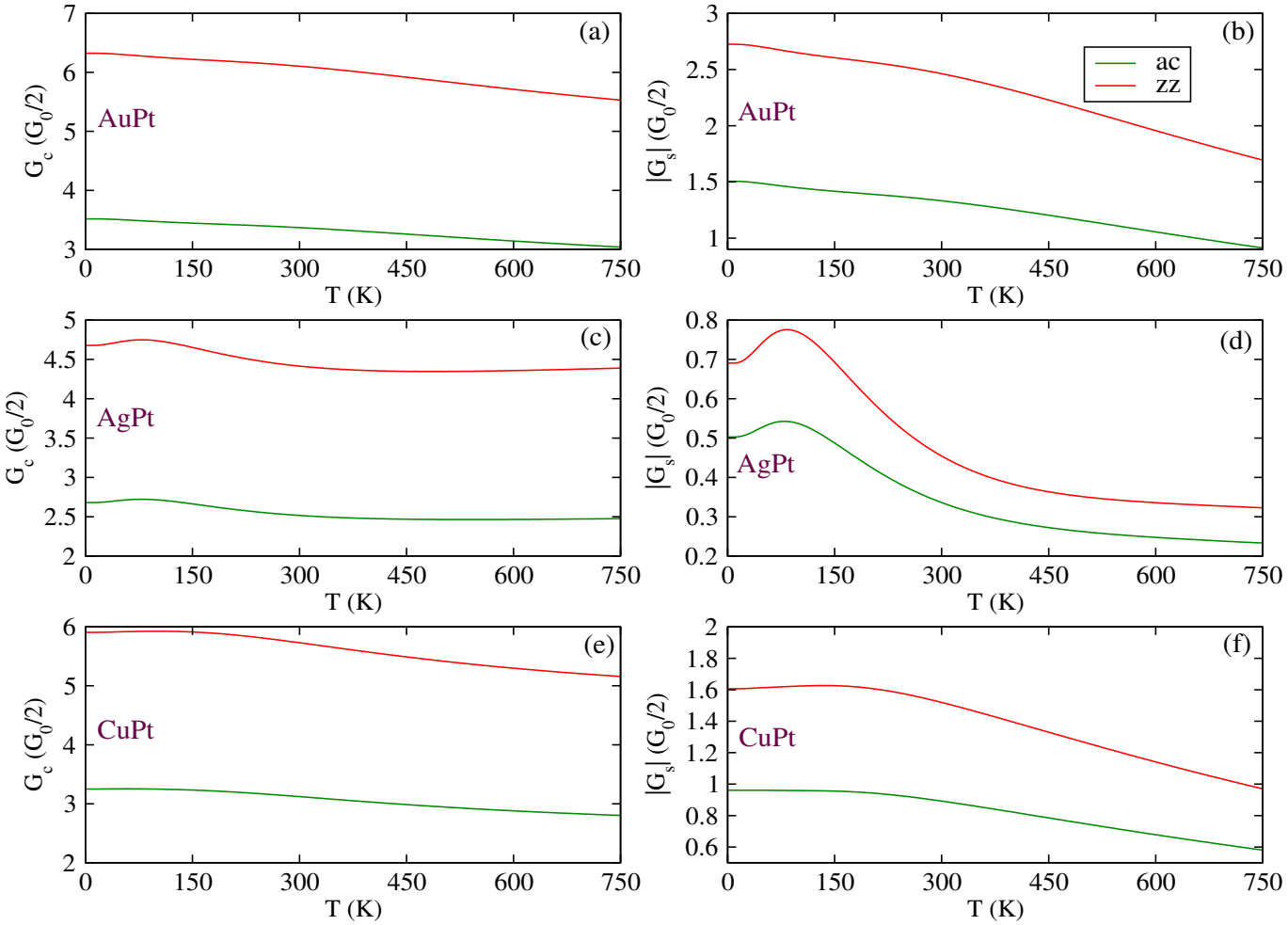

Figure S10 Temperature dependence of charge G_c and spin $|G_s|$ electrical conductance along ac and zz directions for (a-b) AuPt, (c-d) AgPt, and (e-f) CuPt alloyed monolayers.

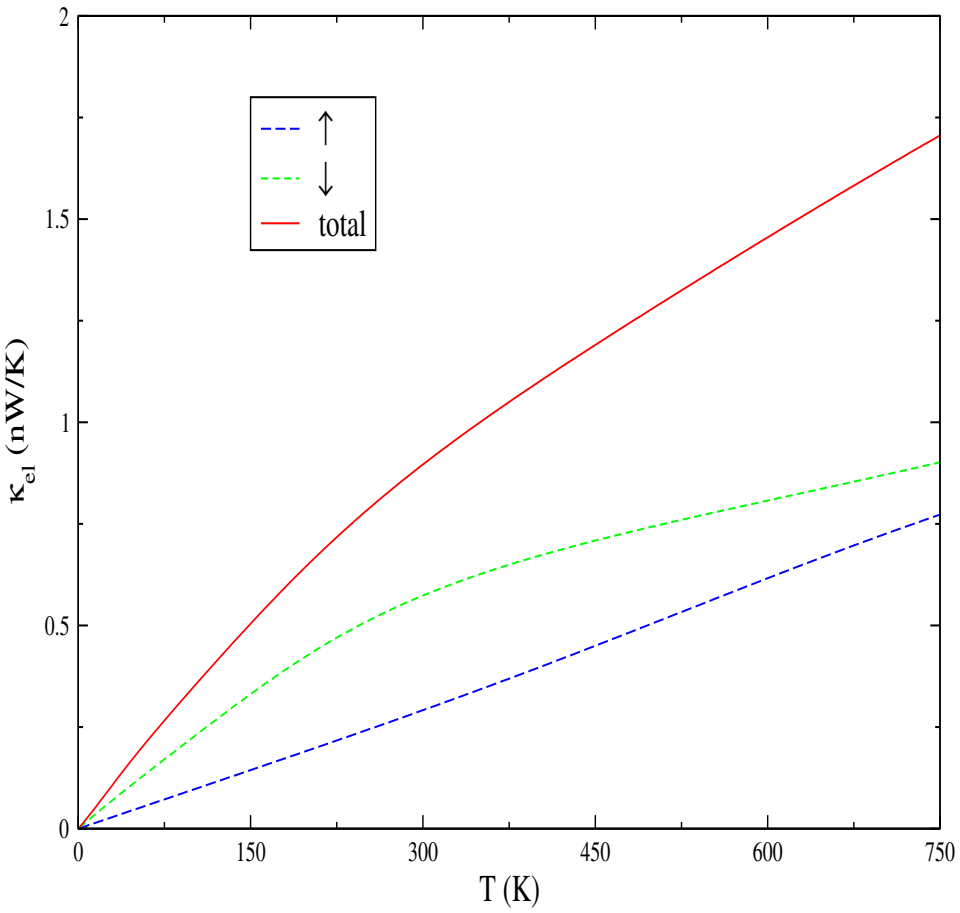

Figure S11 Temperature dependence of total κ_{el} and spin-resolved $\kappa_{el,\sigma}$ electronic thermal conductance in AuPt monolayer for transport in ac-direction.

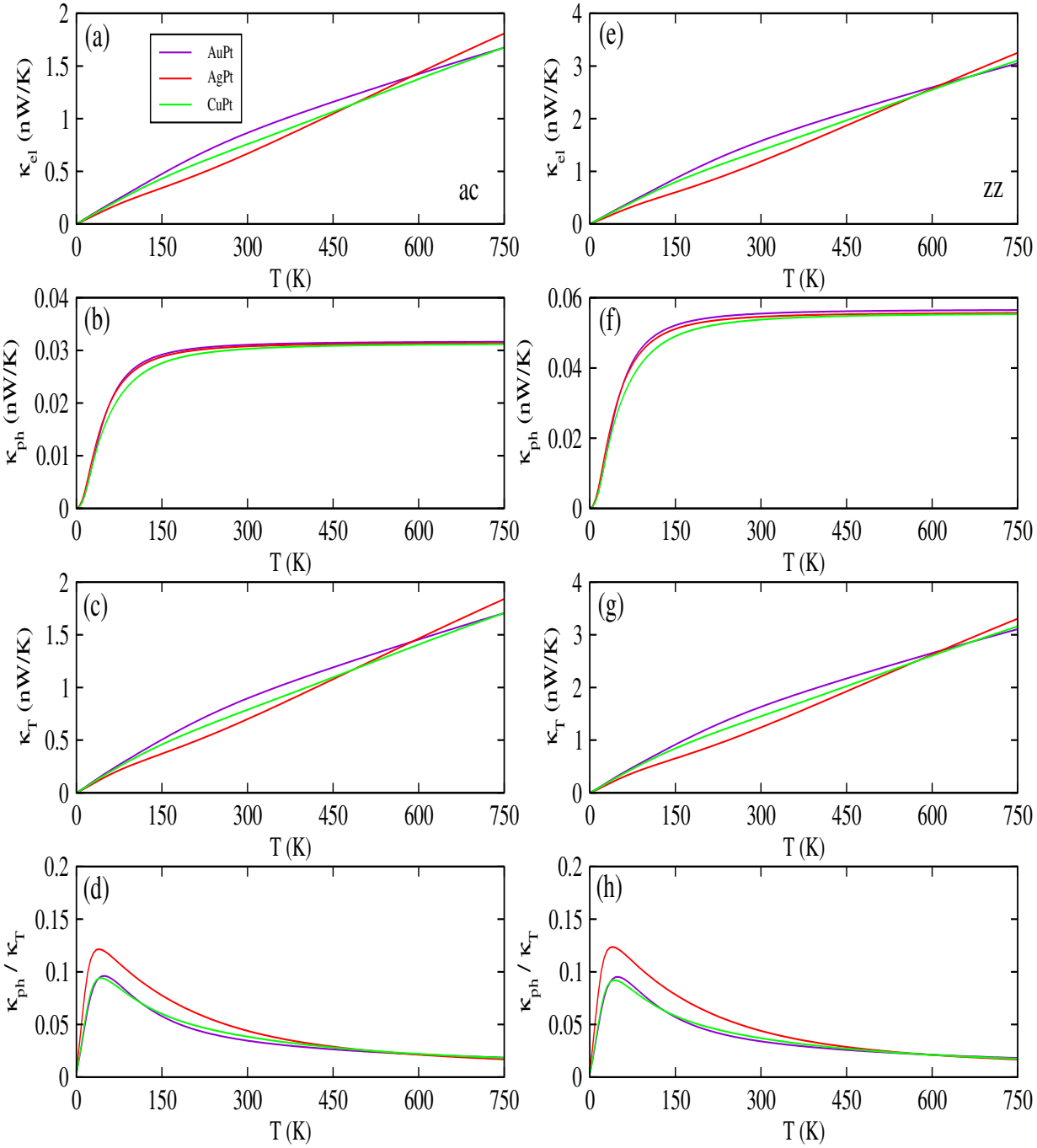

Figure S12 Different thermal transport coefficients: κ_{el}, κ_{ph}, κ_T, and κ_{ph}/κ_T plotted as a function of T in AuPt, AgPt, and CuPt monolayers along ac (a-d) and zz (e-h) directions.

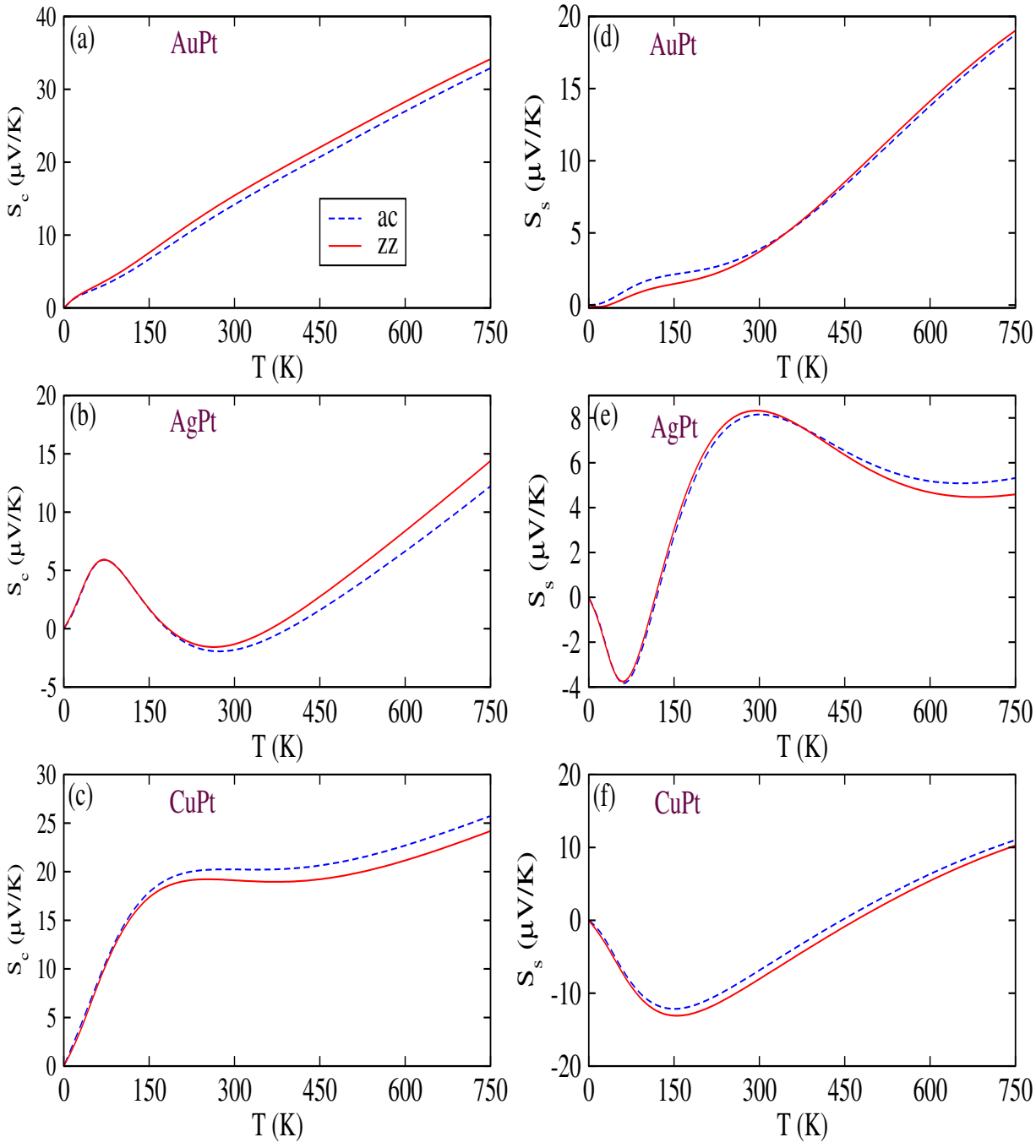

Figure S13 Variation of S_c (a-c) and S_s (d-f) under zero bias for magnetic alloyed monolayers.